Editors' Suggestion | Featured in Physics

Boiling a Unitary Fermi Liquid

Zhenjie Yan,[1] Parth B. Patel,[1] Biswaroop Mukherjee,[1] Richard J. Fletcher,[1] Julian Struck,[1,2] and Martin W. Zwierlein[1]
[1]*MIT-Harvard Center for Ultracold Atoms, Department of Physics, and Research Laboratory of Electronics, Massachusetts Institute of Technology, Cambridge, Massachusetts 02139, USA*
[2]*Département de Physique, Ecole Normale Supérieure/PSL Research University, CNRS, 24 rue Lhomond, 75005 Paris, France*

(Received 1 November 2018; published 6 March 2019)

We study the thermal evolution of a highly spin-imbalanced, homogeneous Fermi gas with unitarity limited interactions, from a Fermi liquid of polarons at low temperatures to a classical Boltzmann gas at high temperatures. Radio-frequency spectroscopy gives access to the energy, lifetime, and short-range correlations of Fermi polarons at low temperatures T. In this regime, we observe a characteristic T^2 dependence of the spectral width, corresponding to the quasiparticle decay rate expected for a Fermi liquid. At high T, the spectral width decreases again towards the scattering rate of the classical, unitary Boltzmann gas, $\propto T^{-1/2}$. In the transition region between the quantum degenerate and classical regime, the spectral width attains its maximum, on the scale of the Fermi energy, indicating the breakdown of a quasiparticle description. Density measurements in a harmonic trap directly reveal the majority dressing cloud surrounding the minority spins and yield the compressibility along with the effective mass of Fermi polarons.

DOI: 10.1103/PhysRevLett.122.093401

Landau's Fermi liquid theory provides a quasiparticle description of the low-temperature behavior for a large class of unordered fermionic states of matter, including most normal metals, atomic nuclei, and liquid helium-3 [1]. Strongly interacting Fermi gases with highly imbalanced spin populations have been identified as belonging to the same class [2–14]. The quasiparticles in spin-imbalanced Fermi gases are Fermi polarons: spin impurities dressed by an excess cloud of majority fermions. The stability of quasiparticles in a Fermi liquid is a consequence of the restricted phase space for collisions due to Pauli blocking. With increasing temperature T, the accessible phase space increases, and the lifetime of quasiparticles shortens, leading to the breakdown of Fermi liquid theory. In this intermediate temperature regime, the gas is neither a Fermi liquid nor a classical Boltzmann gas. For strong interactions, this regime is void of well-defined quasiparticles and controlled by the quantum critical point of the unitary spin-balanced gas at zero chemical potential and temperature [15–17].

Ultracold Fermi gases offer a unique opportunity to study the crossover from a low-temperature Fermi liquid to a classical Boltzmann gas, due to the large accessible temperature range. In spin-imbalanced Fermi gases, the two inequivalent Fermi surfaces provide additional richness. As the temperature is lowered from the classical regime, the Fermi surface of the majority forms first, giving minority spins the quasiparticle character of polarons. At even lower temperatures, the polarons themselves become quantum degenerate and form a Fermi surface.

In this Letter, we access the entire crossover from degenerate polarons to the classical Boltzmann gas through the quantum critical region. The internal properties of the polaronic quasiparticles are measured via radio-frequency (rf) spectroscopy [10,18–20] on a homogeneous Fermi gas [21,22]. At low temperatures, the peak position and width of the rf spectra reflect energy and decay rate of the polarons. Note that the decay rate of a quasiparticle can be viewed as the rate of momentum relaxation in a transport measurement (see, e.g., [7]). The wings of the rf spectra yield information about the short-range correlations and the contact [23–27], controlling the change in the polaron energy with interaction strength. Further thermodynamic properties of the polaron gas are directly obtained from *in situ* density profiles in the presence of a harmonic potential [6,12,13,28–30], revealing the number of atoms in the majority dressing cloud of a polaron. The compressibility of the impurity gas at low temperature yields the effective mass of Fermi polarons.

For the spectroscopic studies we employ rf *ejection* spectroscopy, where the many-body state is first prepared and then probed by transferring a small fraction of one spin component into a weakly or noninteracting final state. Radio-frequency ejection spectroscopy has been used to, e.g., measure interactions, correlations, pairing phenomena in Fermi gases [31,32], and more specifically, the binding energy of the attractive Fermi polaron at low temperatures [10,19]. A prerequisite for our measurements is a spatially uniform box potential. This avoids the spectral broadening caused by an inhomogeneous density and impurity concentration [21,33]. The three energetically lowest hyperfine states of ^{6}Li (labeled $|1\rangle, |2\rangle, |3\rangle$) are utilized to create and probe the strongly interacting spin mixture. The minority

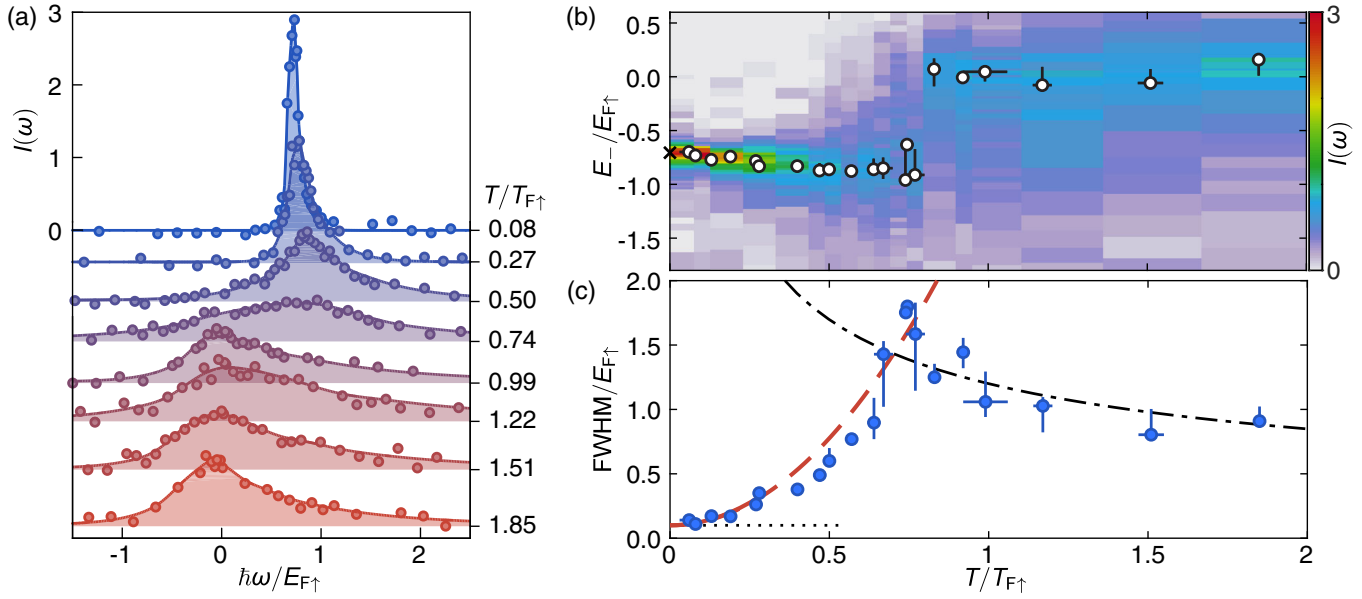

FIG. 1. (a) Thermal evolution of the minority rf spectra. The impurity concentration is $n_\downarrow/n_\uparrow = 0.10 \pm 0.03$, the Rabi frequency $\Omega_R = 2\pi \times 0.5$ kHz, and the pulse duration $T_{\text{pulse}} = 1$ ms. (b) 2D plot of the minority spectra with maxima highlighted by white points. To reflect the energy of the initial many-body state, the spectra are shown with the inverse frequency $E_-/E_{F\uparrow}$, where $E_- = -\hbar\omega$. The cross corresponds to the theoretical zero temperature result for the polaron energy, including a correction for final state interactions [3–5,8,38]. (c) FWHM of the rf spectra. (Dotted line) Fourier resolution limit; (dashed red line) single-polaron decay rate $\Gamma/E_{F\uparrow} = 2.71(T/T_{F\uparrow})^2$ [7], offset by the Fourier limit; (dash-dotted black line) FWHM of the rf spectrum in the high-temperature limit $\Gamma/E_{F\uparrow} = 1.2\sqrt{T_{F\uparrow}/T}$ [40,41], reflecting the scattering rate in the classical, unitary Boltzmann gas. [For the errors in (b) and (c), see the Supplemental Material [33]].

(impurity) and majority components are prepared in $|\downarrow\rangle = |1\rangle$ and $|\uparrow\rangle = |3\rangle$ and transferred via the rf drive into the final state $|f\rangle = |2\rangle$ [33,37]. All measurements have been performed at a magnetic field of 690 G, where the interactions between minority and majority atoms are unitarity limited. Final state interactions are weakly repulsive with $k_{F\uparrow}a_{\uparrow f} \lesssim 0.2$ ($a_{\uparrow f} = 62$ nm). The impurity concentration (minority to majority density ratio $n_\downarrow/n_\uparrow$) is controllably varied between 10% and 30%.

The rf response is linked to the probability that a hole of energy E and momentum $\mathbf{p}$ is excited by ejecting a particle from the many-body state, as described by the occupied spectral function $\mathcal{A}_{-\downarrow}(\mathbf{p}, E)$ [10,32,38,39]. Detecting a free particle of momentum $\mathbf{p}$ after rf transfer implies a momentum $\mathbf{p}$ and energy $E_{\mathbf{p}} = \mathbf{p}^2/2m - \mu_\downarrow - \hbar\omega$ of the leftover hole, where $\mu_\downarrow$ is the minority chemical potential and $\hbar\omega$ is the energy of the rf photon with respect to the noninteracting transition. The number of transferred minority atoms $N_f(\omega)$ is proportional to the momentum integral of the occupied spectral function $\mathcal{A}_{-\downarrow}(\mathbf{p}, E_{\mathbf{p}})$. Fermi liquids feature a spectral function that is sharply peaked around $\epsilon_0 + \mathbf{p}^2/2m^* - \mu_\downarrow$, with the effective mass m^* and dressed energy ϵ_0 of the quasiparticles. The width of the peak is determined by the quasiparticle decay rate $\Gamma(p, T)$. For low temperatures and impurity concentrations, only low-momentum states are populated and the peak position of the rf spectrum corresponds to the polaron binding energy [10].

Figure 1(a) shows the evolution with temperature of the rf spectra. Here, we have defined the normalized transfer $I(\omega) = [N_f(\omega)/N_\downarrow](E_{F\uparrow}/\hbar\Omega_R^2 T_{\text{pulse}})$, with the number of particles in the final (initial) state N_f ($N_\downarrow$), the pulse duration T_{pulse}, and the single particle Rabi frequency Ω_R. The term $\Omega_R^2 T_{\text{pulse}}$ originates from the linear response to the rf pulse. The factor $E_{F\uparrow}/\hbar$ in I is owed to the scale invariance of the unitary Fermi gas, which implies that its spectral features, such as the peak position, amplitude, and width directly scale with the Fermi energy [31,32]. The normalized transfer only depends on the dimensionless parameters $T/T_{F\uparrow}$, $n_\downarrow/n_\uparrow$, and $\hbar\omega/E_{F\uparrow}$, apart from small corrections due to final state interactions and Fourier broadening that break the scale invariance of the system. The energy of the gas is measured by an isoenergetic release from the uniform to a harmonic trap. After thermalization, the in-trap size reveals the energy, from which we obtain the temperature via the equation of state (see Supplemental Material [33]].

In the deeply degenerate limit ($T/T_{F\uparrow} < 0.1$), we observe a sharply defined resonance [Fig. 1(a)] signaling the stable long-lived Fermi polaron [10]. Its width, defined by the full width at half maximum (FWHM), is limited by the Fourier resolution. From the position of the spectral

peak at low temperature [Fig. 1(b)] and correction for weak final state interactions as in [10], we obtain a zero temperature polaron binding energy $A \equiv \epsilon_0/E_{F\uparrow} = -0.60 \pm 0.05$, with a linear extrapolation of the peak positions below $T/T_{F\uparrow} = 0.3$.

With increasing temperature, the spectral peak initially shifts to higher frequencies and broadens significantly [Figs. 1(b) and 1(c)]. A rise in the polaron binding energy with temperature is expected, given the increased scattering phase space of the majority spins, and is found theoretically [42,43]. However, note that the position of the maximum at finite temperature and impurity concentration is influenced by the density of states, the difference in the effective mass between initial and final state [20], and the thermal population of momentum states. At a temperature near $T/T_{F\uparrow} \approx 0.75$, a sharp jump in the position of the global maximum to $\omega \approx 0$ is observed [Figs. 1(a) and 1(b)] [44]. In this regime, the width of the spectra reaches its maximum [Fig. 1(c)], on the order of the Fermi energy. Beyond this temperature, the position of the maximum remains constant at $\omega \approx 0$, as expected theoretically [40,41]. It reflects a merging of attractive and repulsive branches, symmetric about zero on resonance [45], as the temperature exceeds their splitting.

The spectral function of a Fermi liquid is a single Lorentzian peak with a width given by the decay rate of the quasiparticles [1]. The width of the rf spectra is dominated by this decay rate at low temperatures. We observe a quadratic scaling of the width at low temperatures, a hallmark of Fermi liquid theory, in agreement with a theoretical calculation [Fig. 1(c)] [7]. In the quantum critical regime around $T \approx T_{F\uparrow}$, the lifetime of the polarons drops below the Fermi time ($h/E_{F\uparrow}$), signaling a breakdown of quasiparticles [15–17]. The decrease in width at temperatures beyond the Fermi temperature is expected for a classical Boltzmann gas with unitarity limited interactions. The thermal scattering rate in the dilute impurity limit is given by $\Gamma_{\rm th} = n_\uparrow \sigma_{\rm th} v_{\rm th} \sim 1/\sqrt{T}$, with the thermal velocity $v_{\rm th} \sim \sqrt{T}$ and the unitarity limited scattering cross section $\sigma_{\rm th} \sim \lambda^2 \sim 1/T$.

Apart from energies and lifetimes, rf spectra also directly yield the strength of short-range correlations, quantified by contact C [Fig 2(a)] [24–27,31,46,47]. The contact is a central quantity in a set of universal relations, linking microscopic properties to thermodynamics, which apply to all many-body systems with contact interactions [23]. It governs the tail of the momentum distribution, short-range pair correlations, and the change in energy with interaction strength [27,31,32]. As the contact is a measure of pair correlations, the tails of the rf spectrum of the minority and majority components are identical. For unitarity limited interactions, the fraction of transferred atoms in the high-frequency limit is given by [27]

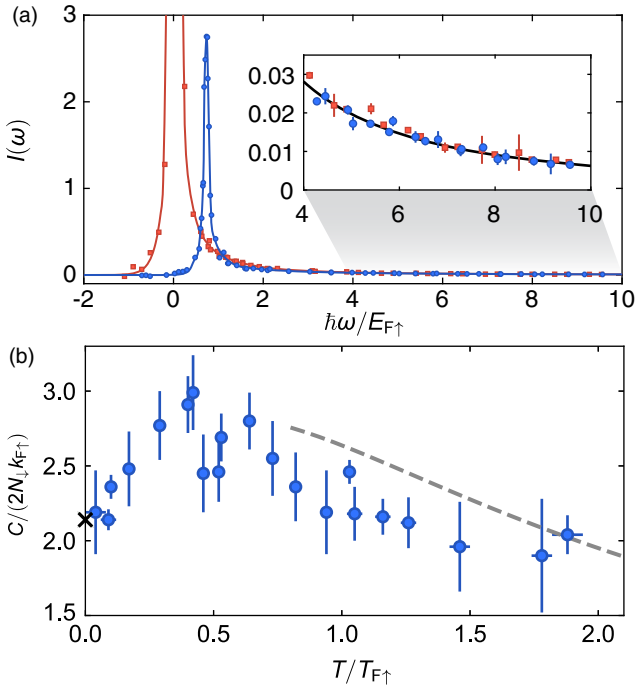

FIG. 2. Contact of the spin-imbalanced Fermi gas. (a) Typical rf spectra of the spin minority (blue circles) and majority (red squares). The impurity concentration is 10%. (Inset) High-frequency tails of the minority and majority spectra together with a fit of Eq. (1). (b) Contact as a function of temperature, obtained by measuring the transferred fraction of atoms as a function of rf pulse duration for frequencies $\hbar\omega/E_{F\uparrow} > 5.5$ and use of Eq. (1). The gray dashed line shows the third-order viral expansion [48] and the cross shows the result from the Chevy ansatz [3,49].

$$I(\omega) \underset{\omega\to\infty}{=} \frac{C}{2N_\downarrow k_{F\uparrow}} \frac{1}{2\sqrt{2}\pi(1+\hbar\omega/E_b)} \left(\frac{E_{F\uparrow}}{\hbar\omega}\right)^{3/2}, \quad (1)$$

where $E_b = \hbar^2/ma_{\uparrow f}^2 \approx h \times 433$ kHz. The inset of Fig. 2(a) shows the corresponding fit of the tails with Eq. (1), leaving only the contact as a free parameter.

The temperature dependence of the contact displays a nonmonotonic behavior with a maximum located around $T \approx 0.4T_{F\uparrow}$ [Fig. 2(b)]. The observed initial rise in temperature is partially expected from the increase in scattering phase space and has also been found theoretically in a spin-imbalanced few-body calculation of the contact [50]. In the high-temperature limit, the contact is proportional to the scattering cross section and vanishes as $1/T$.

The contact quantifies short-range correlations. However, the polaron is an extended object with pair correlations extending out over distances even beyond the majority interparticle spacing [51]. We thus set out to probe the entire cloud of excess majority atoms surrounding the impurity spin of density $\Delta n_\uparrow = n_\uparrow(\mu_\uparrow, \mu_\downarrow, T) - n_0(\mu_\uparrow, T)$ by *in situ* density measurements [Fig. 3(a)]. Here, $n_\uparrow(\mu_\uparrow, \mu_\downarrow, T)$ is the actual measured density of the interacting majority

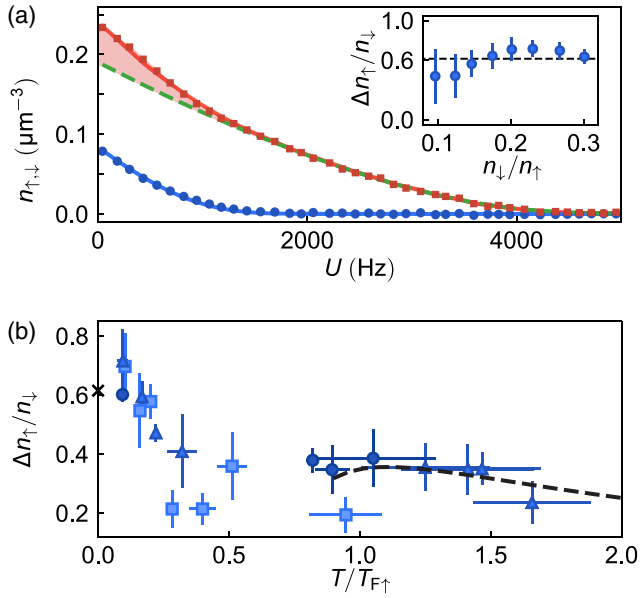

FIG. 3. Observation of the majority excess cloud. (a) Density profiles in a harmonically varying external potential U. Blue (red) data points indicate the profiles of the minority (majority) spin component. The normalized temperature of the gas is $T/T_{F\uparrow} = 0.07$ in the trap center ($U = 0$). The green dashed line represents the equation of state of the ideal Fermi gas, the red (blue) solid line is the Fermi liquid ansatz [Eq. (3)] for the majority (minority) component. The red shaded area displays the excess majority density $\Delta n_\uparrow$. (Inset) Dependence of the excess majority to minority ratio on the impurity concentration. (b) Temperature dependence of the majority excess cloud. Data points show the excess majority density $\Delta n_\uparrow$ for an impurity concentration of $n_\downarrow/n_\uparrow = 0.1$ (squares), $n_\downarrow/n_\uparrow = 0.2$ (triangles), and $n_\downarrow/n_\uparrow = 0.3$ (circles). The cross indicates the low-temperature prediction of the Fermi liquid ansatz $\Delta n_\uparrow/n_\downarrow = -A = 0.615$ [8] and the dashed line shows the third-order virial expansion.

component and $n_0(\mu_\uparrow, T)$ corresponds to the density of a noninteracting gas with the same temperature and majority chemical potential. For this measurement, we use a hybrid trapping potential that is harmonic along one direction and uniform along the other two axes [21]. This trapping geometry gives direct access to the density of each spin component as a function of the trapping potential U [Fig. 3(a)]. Under the local density approximation, the knowledge of $n_{\uparrow,\downarrow}(U)$ can be used to extract a variety of thermodynamic quantities [12,13,30,33]. The majority chemical potential and temperature are obtained from the low-fugacity wings of the gas. In the case of a partially spin polarized wing, we use the third-order virial expansion [48], whereas for a fully spin polarized wing, we use the ideal equation of state. For the lowest temperatures, the excess majority density per minority atom is $\Delta n_\uparrow/n_\downarrow = 0.63(5)$ [Fig. 3(b)]. For increasing temperature, the excess density drops until it reaches the value predicted by the virial expansion for the density. $\Delta n_\uparrow/n_\downarrow$ displays no dependency on the minority concentration within our error up to $n_\downarrow/n_\uparrow = 0.3$.

To elucidate the origin of the excess density from thermodynamics, we model the total pressure of the system as

$$P(\mu_\uparrow, \mu_\downarrow, T) = P_0(\mu_\uparrow, T) + \left(\frac{m^*}{m}\right)^{\frac{3}{2}} P_0(\mu_\downarrow - A\mu_\uparrow, T). \quad (2)$$

Here, $P_0(\mu, T)$ is the pressure of the noninteracting Fermi gas. The ansatz describes the total pressure of the system as the sum of the partial pressure of the noninteracting majority component and the partial pressure of an ensemble of polarons with an effective chemical potential of $\mu_\downarrow - A\mu_\uparrow$ and an effective mass m^* [12,13]. It contains weak interactions among the polarons that amount to a few percent of the total energy of the system [52]. From this pressure ansatz, the density can be calculated with the Gibbs-Duhem equation at constant temperature and scattering length ($dP = n_\uparrow d\mu_\uparrow + n_\downarrow d\mu_\downarrow$),

$$\begin{aligned} n_\uparrow(\mu_\uparrow, \mu_\downarrow, T) &= n_0(\mu_\uparrow, T) - A n_\downarrow(\mu_\uparrow, \mu_\downarrow, T), \\ n_\downarrow(\mu_\uparrow, \mu_\downarrow, T) &= (m^*/m)^{\frac{3}{2}} n_0(\mu_\downarrow - A\mu_\uparrow, T), \end{aligned} \quad (3)$$

where $n_0(\mu, T) \equiv \partial P_0/\partial\mu$ is the density of the noninteracting gas. Each minority is accumulating on average $|A| = 0.6$ excess majority atoms over the noninteracting limit, in agreement with our measured value [Fig. 3(b)].

Since the Fermi liquid ansatz describes the thermodynamics accurately in the low-temperature regime $T/T_{F\uparrow} < 0.2$, we now focus on this temperature regime and utilize the ansatz to determine the effective mass of the polarons from a measurement of the minority compressibility. In analogy to the total compressibility of the gas, the normalized isothermal minority compressibility is defined as $\tilde{\kappa}_\downarrow \equiv -dE_{F\downarrow}/dU_{\text{eff}}$ [30]. Here, $U_{\text{eff}} = (1 - A)U$ is the effective potential of the minority component generated by the interaction with the majority component [4,11]. Using Eq. (3) for the minority density, one finds

$$\tilde{\kappa}_\downarrow(T/T_{F\downarrow}) = \frac{m^*}{m} \frac{\kappa_0(T, T_{F\downarrow} m^*/m)}{\kappa_0(0, T_{F\downarrow} m^*/m)}, \quad (4)$$

where $\kappa_0(T, T_{F\downarrow}) \equiv n_0^{-2}(\partial n_0/\partial\mu)_T$ is the compressibility of the noninteracting Fermi gas at fixed density. Figure 4 shows the measured isothermal compressibility of the minority component. A fit of Eq. (4) fixing $A = -0.615$ [8] results in an effective mass of $m^*/m = 1.25(5)$, which is in agreement with results obtained from diagrammatic Monte Carlo simulations [8], a variational ansatz [5], and previous low-temperature experiments [11–13]. The saturation of the minority compressibility at low temperatures signals the formation of a degenerate Fermi sea of polarons.

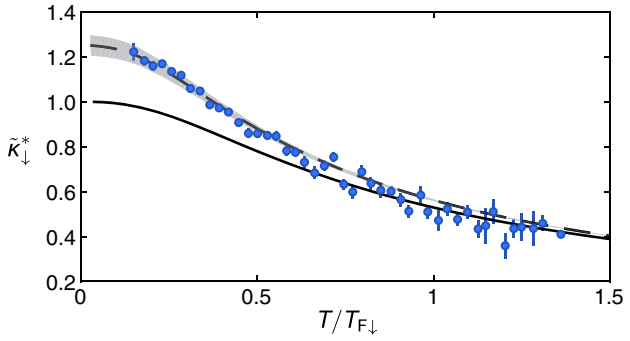

FIG. 4. Isothermal minority compressibility. The solid line is the Fermi liquid ansatz for $m^*/m = 1$, while the dashed line corresponds to a fit with an effective mass of $m^*/m = 1.25(5)$ assuming $A = -0.615$ [8]. The gray shaded area represents the standard deviation of the fit. For the entire range of temperatures displayed, the majority component is degenerate ($T/T_{F\uparrow} < 0.2$).

In conclusion, we have studied the temperature dependence of a highly spin-imbalanced unitary Fermi gas with rf spectroscopy and in-trap density profiles. When the majority component is degenerate ($T/T_{F\uparrow} \ll 1$), long-lived quasiparticles emerge. In the spirit of Fermi liquid theory, these polarons behave like a weakly interacting Fermi gas forming a sharp Fermi sea for $T/T_{F\downarrow} \ll 1$. The weakly interacting character of the quasiparticles is also reflected in the independence of the majority dressing cloud on the impurity concentration. In the opposing high-temperature regime, the gas is accurately described as a classical Boltzmann gas. At intermediate temperatures ($T \approx T_{F\uparrow}$) the quasiparticle description breaks down. The spectral features of the attractive polarons dissolve, merging with excited branches, such as dressed dimerons [8,49,53] and repulsive polarons [18–20,38,53,54].

We thank Richard Schmidt and Felix Werner for helpful discussions. This work was supported by the National Science Foundation (Center for Ultracold Atoms Awards No. PHY-1734011 and No. PHY-1506019), Air Force Office of Scientific Research (FA9550-16-1-0324 and MURI Quantum Phases of Matter FA9550-14-1-0035), Office of Naval Research (N00014-17-1-2257) and the David and Lucile Packard Foundation. J. S. was supported by LabEX ENS-ICFP: ANR-10-LABX-0010/ANR-10-IDEX-0001-02 PSL*.

[1] P. Nozières and D. Pines, *The Theory of Quantum Liquids, Vol. I: Normal Fermi Liquids*, 1st ed. (W.A. Benjamin, New York, 1966).
[2] M. W. Zwierlein, A. Schirotzek, C. H. Schunck, and W. Ketterle, Science **311**, 492 (2006).
[3] F. Chevy, Phys. Rev. A **74**, 063628 (2006).
[4] C. Lobo, A. Recati, S. Giorgini, and S. Stringari, Phys. Rev. Lett. **97**, 200403 (2006).
[5] R. Combescot, A. Recati, C. Lobo, and F. Chevy, Phys. Rev. Lett. **98**, 180402 (2007).
[6] Y.-I. Shin, C. H. Schunck, A. Schirotzek, and W. Ketterle, Nature (London) **451**, 689 (2008).
[7] G. M. Bruun, A. Recati, C. J. Pethick, H. Smith, and S. Stringari, Phys. Rev. Lett. **100**, 240406 (2008).
[8] N. Prokof'ev and B. Svistunov, Phys. Rev. B **77**, 020408 (2008).
[9] M. Veillette, E. G. Moon, A. Lamacraft, L. Radzihovsky, S. Sachdev, and D. E. Sheehy, Phys. Rev. A **78**, 033614 (2008).
[10] A. Schirotzek, C.-H. Wu, A. Sommer, and M. W. Zwierlein, Phys. Rev. Lett. **102**, 230402 (2009).
[11] S. Nascimbène, N. Navon, K. J. Jiang, L. Tarruell, M. Teichmann, J. McKeever, F. Chevy, and C. Salomon, Phys. Rev. Lett. **103**, 170402 (2009).
[12] S. Nascimbène, N. Navon, K. J. Jiang, F. Chevy, and C. Salomon, Nature (London) **463**, 1057 (2010).
[13] N. Navon, S. Nascimbène, F. Chevy, and C. Salomon, Science **328**, 729 (2010).
[14] A. Sommer, M. Ku, and M. W. Zwierlein, New J. Phys. **13**, 055009 (2011).
[15] P. Nikolić and S. Sachdev, Phys. Rev. A **75**, 033608 (2007).
[16] T. Enss, Phys. Rev. A **86**, 013616 (2012).
[17] B. Frank, J. Lang, and W. Zwerger, ZhETF **154**, 953 (2018) [J. Exp. Theor. Phys. **127**, 812 (2018)].
[18] C. Kohstall, M. Zaccanti, M. Jag, A. Trenkwalder, P. Massignan, G. M. Bruun, F. Schreck, and R. Grimm, Nature (London) **485**, 615 (2012).
[19] M. Koschorreck, D. Pertot, E. Vogt, B. Fröhlich, M. Feld, and M. Köhl, Nature (London) **485**, 619 (2012).
[20] F. Scazza, G. Valtolina, P. Massignan, A. Recati, A. Amico, A. Burchianti, C. Fort, M. Inguscio, M. Zaccanti, and G. Roati, Phys. Rev. Lett. **118**, 083602 (2017).
[21] B. Mukherjee, Z. Yan, P. B. Patel, Z. Hadzibabic, T. Yefsah, J. Struck, and M. W. Zwierlein, Phys. Rev. Lett. **118**, 123401 (2017).
[22] K. Hueck, N. Luick, L. Sobirey, J. Siegl, T. Lompe, and H. Moritz, Phys. Rev. Lett. **120**, 060402 (2018).
[23] S. Tan, Ann. Phys. (Amsterdam) **323**, 2971 (2008).
[24] G. Baym, C. J. Pethick, Z. Yu, and M. W. Zwierlein, Phys. Rev. Lett. **99**, 190407 (2007).
[25] M. Punk and W. Zwerger, Phys. Rev. Lett. **99**, 170404 (2007).
[26] W. Schneider, V. B. Shenoy, and M. Randeria, arXiv: 0903.3006.
[27] E. Braaten, D. Kang, and L. Platter, Phys. Rev. Lett. **104**, 223004 (2010).
[28] Y.-I. Shin, Phys. Rev. A **77**, 041603 (2008).
[29] M. Horikoshi, S. Nakajima, M. Ueda, and T. Mukaiyama, Science **327**, 442 (2010).
[30] M. J. H. Ku, A. T. Sommer, L. W. Cheuk, and M. W. Zwierlein, Science **335**, 563 (2012).
[31] M. W. Zwierlein, in *Novel Superfluids*, edited by K.-H. Bennemann and J. B. Ketterson, 1st ed. (Oxford University Press, New York, 2014), Vol. 2, Chap. 18, pp. 269–422.
[32] W. Zwerger, in Quantum Matter at Ultralow Temperatures, *Proceedings of the International School of Physics "Enrico Fermi," Course CXCI*, edited by M. Inguscio, W. Ketterle,

S. Stringari, and G. Roati (IOS Press, Amsterdam, 2016), Chap. 2, pp. 63–142.
[33] See Supplemental Material at http://link.aps.org/supplemental/10.1103/PhysRevLett.122.093401 for more information regarding the homogeneity of the gas, state preparation, thermometry, and rf spectroscopy, which includes Refs. [34–36].
[34] J. E. Thomas, J. Kinast, and A. Turlapov, Phys. Rev. Lett. **95**, 120402 (2005).
[35] T. L. Ho, Phys. Rev. Lett. **92**, 090402 (2004).
[36] S. Nascimbène, N. Navon, S. Pilati, F. Chevy, S. Giorgini, A. Georges, and C. Salomon, Phys. Rev. Lett. **106**, 215303 (2011).
[37] C. H. Schunck, Y.-I. Shin, A. Schirotzek, and W. Ketterle, Nature (London) **454**, 739 (2008).
[38] P. Massignan, M. Zaccanti, and G. M. Bruun, Rep. Prog. Phys. **77**, 034401 (2014).
[39] P. Törmä, Phys. Scr. **91**, 043006 (2016).
[40] T. Enss, R. Haussmann, and W. Zwerger, Ann. Phys. (Amsterdam) **326**, 770 (2011).
[41] M. Sun and X. Leyronas, Phys. Rev. A **92**, 053611 (2015).
[42] H. Tajima and S. Uchino, New J. Phys. **20**, 073048 (2018).
[43] B. C. Mulkerin, X.-J. Liu, and H. Hu, arXiv:1808.07671.
[44] Recently, a preprint appeared in which the authors, motivated by our work, found similar sudden shifts of the peak rf transfer. See H. Tajima and S. Uchino, arXiv:1812.05889.
[45] T. L. Ho and E. J. Mueller, Phys. Rev. Lett. **92**, 160404 (2004).
[46] P. Pieri, A. Perali, and G. C. Strinati, Nat. Phys. **5**, 736 (2009).
[47] J. T. Stewart, J. P. Gaebler, T. E. Drake, and D. S. Jin, Phys. Rev. Lett. **104**, 235301 (2010).
[48] X.-J. Liu and H. Hu, Phys. Rev. A **82**, 043626 (2010).
[49] M. Punk, P. T. Dumitrescu, and W. Zwerger, Phys. Rev. A **80**, 053605 (2009).
[50] Y. Yan and D. Blume, Phys. Rev. A **88**, 023616 (2013).
[51] C. Trefzger and Y. Castin, Europhys. Lett. **101**, 30006 (2013).
[52] C. Mora and F. Chevy, Phys. Rev. Lett. **104**, 230402 (2010).
[53] R. Schmidt and T. Enss, Phys. Rev. A **83**, 063620 (2011).
[54] R. Schmidt, M. Knap, D. A. Ivanov, J.-S. You, M. Cetina, and E. Demler, Rep. Prog. Phys. **81**, 024401 (2018).